Decomposition of HMX at Extreme Conditions: A Molecular Dynamics Simulation

M. Riad Manaa,*,† Laurence E. Fried,† Carl F. Melius,† Marcus Elstner,‡ and Th. Frauenheim‡

Lawrence Livermore National Laboratory, Energetic Materials Center, University of California, P.O. Box 808, L-282, Livermore, California, 94551, and Fachbereich Physik, Theoretische Physik, Universität Paderborn, D-33098 Paderborn, Germany

Received: February 20, 2002; In Final Form: June 3, 2002

We present the results of a quantum molecular dynamics simulation of the chemistry of HMX, a high performance explosive, at a density of 1.9 g/cm^3 and temperature of 3500 K, conditions roughly similar to the Chapman−Jouget detonation state. The molecular forces are determined using the self-consistent-charge density-functional-based tight-binding method. Following the dynamics for a time scale of up to 55 ps allows the construction of effective rate laws for typical products such as H_2O, N_2, CO_2, and CO. We estimate reaction rates for these products of 0.48, 0.08, 0.05, and 0.11 ps^{-1}, respectively. We also find reasonable agreement for the concentrations of dominant species with those obtained from thermodynamic calculations, despite the vastly different theoretical underpinning of these methodologies.

I. Introduction

Detailed description of the chemical reaction mechanisms of condensed energetic materials at high densities and temperatures is essential for understanding events that occur at the reactive front of these materials under combustion or detonation conditions. Under shock conditions, for example, energetic materials undergo rapid heating to a few thousand degrees and are subjected to a compression of hundreds of kilobars,[1] resulting in almost 30% volume reduction. Complex chemical reactions are thus initiated, in turn releasing large amounts of energy to sustain the detonation process. A dense, highly reactive, supercritical fluid is established behind the detonation front. Clearly, understanding the various chemical events at these extreme conditions is essential to build predictive models of material properties that can be incorporated into full continuum approaches of describing the detonation process at the macroscopic level. In this work, we report the results of high-density (1.9 g/cm^3), high-temperature (3500 K) quantum mechanical based molecular dynamics simulation of HMX (1,3,5,7-tetranitro-1,3,5,7-tetraazacyclooctane, Figure 1), a material that is widely used as an ingredient in various explosives and propellants. HMX is a molecular solid at standard state. In our simulations, we study the reactivity of dense fluid (supercritical) HMX at 3500 K. To our knowledge, this is the first reported ab initio based/molecular dynamics study of an explosive material at extreme conditions for extended reaction times of up to 55 ps, thus allowing the formation of stable product molecules.

Experimental characterizations at low temperatures (i.e., <1000 K, well below detonation temperature) of decomposition products of condensed-phase HMX have been numerous.[2−12] These studies tend to identify final gas products (such as H_2O, N_2, H_2, CO, CO_2, etc.) from the surface burn and aspire to establish a global decomposition mechanism. The early thermal decomposition study using mass spectrometry at $T = 503$, 527, and 553 K of Syryanarayana et al.[2a] identified a concerted decomposition into four methylenenitramine ($CH_2N_2O_2$), which can further decompose into CH_2O and N_2O. At 448−548 K, Farber and Srivastava[3] identified a major decomposition product with $m/e = 148$ and proposed a homolytic cleavage of HMX to two $C_2H_4N_4O_4$ fragments that might further decompose to form methylenenitramine via $C_2H_4N_4O_4 \rightarrow 2CH_2N_2O_2$. CH_2N and NO_2 were later detected as decomposition products from the $CH_2N_2O_2$ intermediate in an electron spin resonance pyrolysis study.[4] Recent experiments using thermogravimetric modulated beam mass spectrometry and isotope scrambling identified gaseous pyrolysis products such as H_2O, HCN, CO, CH_2O, NO, and N_2O between 483 and 508 K.[6−8] Brill et al. have analyzed rate measurements for the early stage of HMX thermal decomposition,[10a] revealing the existence of an approximate linear relationship between the Arrhenius prefactor,

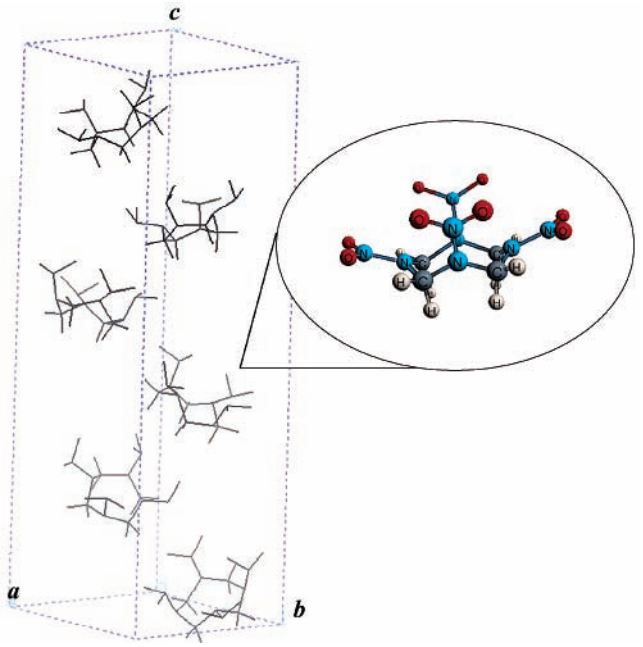

Figure 1. Crystal and molecular (insert) configurations of HMX in the δ phase.

* Corresponding author. E-mail: manaa1@llnl.gov.
† University of California.
‡ Universität Paderborn.

10.1021/jp025668+ CCC: $22.00
Published on Web 08/30/2002

ln A, and the apparent activation energy, E_a. Brill later suggested[10b] two competing global mechanisms for thermal decomposition, the first leading to 4HONO and 4HCN, and the second leading to the formation of $4CH_2O$ and $4N_2O$.

The above-noted experimental work on thermal decomposition of condensed phase HMX is largely restricted to relatively low temperature (~550 K) and pressure (0.1 GPa) regimes. Similar experimental observations at detonation conditions (temperatures 2000−5000 K and pressure 10−30 GPa), however, have not been realized to date. Although recent applications of ultrafast spectroscopic methods[13] hold great promise for determining such decomposition mechanisms in the foreseeable future, at present, computer simulations provide the best access to the short time scale processes occurring in these regions of extreme conditions of pressure and temperature. The use of ab initio/molecular dynamics has been successfully demonstrated recently for water, ammonia, and methane at temperatures up to 7000 K and pressures of up to 300 GPa.[14,15] Though the application of these methods to large molecular systems for several tens of picoseconds is currently prohibitive, tight-binding methods emerge as viable tools, as has been recently demonstrated in the studies of shocked hydrocarbons.[16,17]

Previous theoretical studies have included electronic structure calculations of various decomposition channels of the gas-phase HMX molecule.[18−20] Melius used the bond-additivity-corrected (BAC) MP4 method to determine decomposition pathways for nitramine compounds, HMX and RDX.[18] The initial step in his decomposition scheme is $N-NO_2$ bond breaking, which subsequently causes a significant weakness in the second-nearest-neighbor bond breaking energies (18 kcal/mol for the C−N bond dissociation), leading to HCN, NO_2, and H as the net products for rapid thermal heating. In the condensed phase, however, Melius made the observation that alternative decomposition mechanisms can occur. The deposed NO_2 fragment can recombine as a nitride, which can then decompose by breaking the O−N bond to form NO, or attract weakly hydrogen atoms and form HONO. The HONO molecules can then rapidly equilibrate to form water via the reaction $2HONO \rightarrow H_2O + NO_2 + NO$.

Lewis et al.[19] calculated four possible decomposition pathways of the α-HMX polymorph: $N-NO_2$ bond dissociation, HONO elimination, C−N bond scission, and the concerted ring fission. On the basis of the energetics, it was determined that $N-NO_2$ dissociation was the initial mechanism of decomposition in the gas phase, whereas they proposed HONO elimination and C−N bond scission to be favorable in the condensed phase. The more recent study of Chakraborty et al.,[20] using the DFT-(B3LYP) method, reported detailed decomposition pathways of the β-HMX, the stable polymorph at room temperature. It was concluded that consecutive HONO elimination (4HONO) and subsequent decomposition into HCN, OH, and NO are energetically the most favorable pathways in the gas phase. The results also showed that the formation of CH_2O and N_2O could occur preferably from secondary decomposition of methylenenitramine. Whereas these studies concentrated on gas-phase decomposition mechanisms, to date no computational treatment of condensed phase reaction mechanisms exist. Other theoretical studies were concerned with the derivation of a force field from first principle calculations,[21] and the application of classical molecular dynamics as in simulating pressure effects on crystal packing.[22,23]

In this work, we use the self-consistent-charge density-functional tight-binding (SCC-DFTB) method[24−26] to determine the interatomic forces and simulate the decomposition of HMX at constant-volume and -temperature conditions. This method is an extension of the standard tight-binding approach in the context of density functional theory, allowing for the description of total energies, atomic forces, and charge transfer in a self-consistent manner. The method has been successfully tested on organic molecules and biomolecules[27,28] and has been shown to accurately predict reaction energies.[25] We expect that the accuracy of this technique when applied to nitramines is similar to that of other materials. Validations of the method by comparison to existing experiments and independent computational approaches are performed below. Future experiments at comparable conditions, however, will be necessary to unambiguously ascertain the accuracy of our simulations. In section II, we provide the computational treatment for our simulation, including a description of the SCC-DFTB method. Section III presents and discusses the results, and section IV summarizes and outlines our future work.

II. Computational Approach

The interatomic forces that are needed to solve Newton's equations of motion are calculated using the SCC-DFTB method. Although this method has been presented elsewhere, its use in the present context of high-pressure reactivity is new. We thus provide a brief outline of the underlying formulation of this method. SCC-DFTB is based on a second-order expansion of the Kohn−Sham energy functional from DFT with respect to charge density fluctuations $\delta n(\mathbf{r})$ relative to a reference density $n_0(\mathbf{r})$:

$$E_{\mathrm{DFT}} = \sum_{i}^{\mathrm{occ}} n_i \langle \psi_i | \hat{H}^0 | \psi_i \rangle + E_{\mathrm{rep}}[n_0] + \Delta E^{(2)} \qquad (1)$$

$\hat{H}^0$ is the single-particle Hamiltonian operator resulting from the density n_0, and ψ_i represents the single-particle electron wave functions corresponding to valence states. The second term, E_{rep}, represents the ion−ion short-range repulsion represented by an effective pair potential.[29] The second-order term, ΔE^2, is given by a simple distribution of atom-centered point charges:

$$\Delta E^{(2)} = \frac{1}{2} \sum_{\alpha\beta} \gamma_{\alpha\beta} \Delta q_\alpha \Delta q_\beta \qquad (2)$$

where $\Delta q_\alpha = q_\alpha - q_\alpha^0$ are the atom-centered charge density fluctuations in the usual Mulliken charge analysis. This term explicitly accounts for the long-range interatomic Coulomb interactions between point charges at different sites under the monopole approximation and includes the self-interaction contributions of single atoms.[25] For large distances, the interaction integrals $\gamma_{\alpha\beta}$ reduce to the Coulombic form, whereas at intermediate distances, they incorporate screening effects and approximate the chemical hardness of the single atoms on-site terms, $\gamma_{\alpha\alpha}$.

The single-particle functions, $\psi_i = \psi_i(r)$, are expanded in a suitable set of linear combination of nonorthogonal atomic orbitals φ_ν,

$$\psi_i(r) = \sum_{\nu(\alpha)} c_{\nu i} \varphi_\nu (r - R_\alpha) \qquad (3)$$

Applying the variational minimization of the approximate Kohn−Sham energy, including normalization constraints, results in a set of equations of the form

$$\sum_{\nu}^{M} c_{\nu i} (H_{\mu\nu} - \epsilon_i S_{\mu\nu}) = 0 \qquad (4)$$

which are self-consistent through the modification of the Hamiltonian matrix elements due to the nonzero term of $\Delta E^{(2)}$. We further use a DFT-based two-center construction for the Hamiltonian and overlap integrals along with the repulsive interactions $E_{rep}(n_0)$ as a function of distance. As such, the SCC-DFTB method allows for improved accuracy and chemical transferability over standard tight-binding schemes. For the system of interest, HMX, the tight-binding overlap integrals have been evaluated for the requisite C, N, O, and H atom types. A minimal basis set of one s orbital on hydrogen and s and p orbitals on carbon, nitrogen, and oxygen was employed.

The initial condition of the simulation included six HMX molecules in a cell, corresponding to the unit cell of the δ phase of HMX (Figure 1) with a total of 168 atoms. It is well-known[30] that HMX undergoes a phase transition at 436 K from the β phase (two molecules per unit cell with a chair molecular conformation, density = 1.89 g/cm^3) to the δ phase (with boat molecular conformation, density = 1.50 g/cm^3). We thus chose the δ phase as the initial starting structure so as to include all the relevant physical attributes of the system prior to chemical decomposition. The calculation started with the experimental unit cell parameters and atomic positions of δ HMX. The atomic positions were then relaxed in an energy minimization procedure. The resulting atomic positions were verified to be close to the experimental positions.

The volume of the cell was then reduced to the final density of the simulation. The atomic structure was subsequently fully optimized at the corresponding cell volume. Our intention is to study the high-pressure and high-temperature chemistry of HMX in general, so the exact density and temperature used in our simulation is somewhat arbitrary. We used a density of 1.9 g/cm^3 and a temperature of 3500 K. This state could be achieved through a sudden heating of HMX in a diamond anvil cell under constant volume conditions.

Although we do not study shocks here, we discuss the current simulation in the context of shock processes, because similar conditions are achieved in shocks or detonations. The studied state is in the neighborhood of the Chapman−Jouget state of β-HMX (3500 K, 2.1 g/ cm^3), as predicted through thermochemical calculations described later. The Chapman−Jouget state is achieved behind a steady detonation front when the material has fully reacted. The studied state is significantly hotter and less dense than the von Neumann state of HMX (1400 K, 2.8 g/ cm^3), as predicted through thermochemical calculations. The von Neumann state is achieved when a steady detonation wave encounters unreacted material. Because our simulation was performed at a much higher temperature than that state, the calculated reaction rates would likely be much faster than those experienced during an actual detonation. The closest experimental condition corresponding to our simulation would be a sample of HMX, which is suddenly heated under constant volume conditions, such as in a diamond anvil cell.

The molecular dynamics simulation was conducted at constant volume and constant temperature. Periodic boundary conditions, whereby a particle exiting the cell on one side is reintroduced on the opposing side with the same velocity were imposed. Constant temperature conditions were implemented through simple velocity rescaling. The probability to rescale atom velocities was chosen to be 0.1 per time step. A dynamic time step of 0.5 fs was used, and snapshots at 2.5 fs steps were collected.

A procedure was implemented to identify the product molecules of interest: H_2O, N_2, CO_2, and CO. Covalent bonds were identified according to bond distance. This is motivated by the difference between covalent (1−1.7 Å) and van der Waals bond distances (∼3 Å). We chose maximum bond distances of R(O−H) = 1.3, R(CO) = 1.7, and N−N = 1.5 Å in the molecule identification procedure. The results of the molecular identification procedure were confirmed through visual examination of representative simulation steps. We note that the procedure may incorrectly identify transition states as being molecular species. Because transition states are short-lived, and because we apply the procedure to small molecules, this problem should not significantly affect the time averaged concentrations reported here.

III. Results and Discussion

We first discuss the overall chemical process predicted, followed by a discussion of reaction mechanisms. Under the simulation conditions, the HMX was in a highly reactive dense fluid phase. There are important differences between the dense fluid (supercritical) phase and the solid phase, which is stable at standard conditions. Namely, the dense fluid phase cannot accommodate long-lived voids, bubbles, or other static defects, because it has no surface tension. Instead, numerous fluctuations in the local environment occur within a time scale of tens of femtoseconds. The fast reactivity of the dense fluid phase and the short spatial coherence length make it well suited for molecular dynamics study with a finite system for a limited period of time. Under the simulation conditions chemical reactions occurred within 50 fs. Stable molecular species were formed in less than 1 ps. We report the results of the simulation for up to 55 ps. Parts a−d of Figure 2 display the product formation of H_2O, N_2, CO_2, and CO, respectively. The concentration, $C(t)$, is represented by the actual number of product molecules formed at the corresponding time t. Each point on the graphs (open circles) represents a 250 fs averaged interval. The number of the molecules in the simulation was sufficient to capture clear trends in the chemical composition of the species studied. These concentrations were in turn fit to an expression of the form: $C(t) = C_\infty(1 - e^{-bt})$, where C_∞ is the equilibrium concentration and b is the effective rate constant. From this fit to the data, we estimate effective reaction rates for the formation of H_2O, N_2, CO_2, and CO to be 0.48, 0.08, 0.05, and 0.11 ps^{-1}, respectively.

It is not surprising that the rate of H_2O formation is much faster than that of N_2. Fewer reaction steps are required to produce a triatomic species such as water, whereas the formation of N_2 involves a much more complicated mechanism.[18] Further, the formation of water (Figure 2a) starts around 0.5 ps and seems to have reached a steady state at 10 ps, with oscillatory behavior of decomposition and formation clearly visible. We expect this trend to continue until chemical equilibrium is reached, well beyond the current simulation time. The formation of N_2 (Figure 2b), on the other hand, starts around 1.5 ps and is still progressing (slope of the graph is slightly positive) after 55 ps of simulation time, albeit at small variation.

Due to the lack of high-pressure experimental reaction rate data for this (and other) explosive(s) with which to compare, we produce in Figure 3 a comparison of dominant species formation for decomposing HMX obtained from an entirely different theoretical approach. The concentration of species at chemical equilibrium can be estimated through thermodynamic calculations. Molecules are modeled as a soft sphere fluid mixture interacting through an exponential-6 potential. The equation of state of the soft sphere fluid has been determined through a combination of integral theory and Monte Carlo calculations.[31] Condensed carbon is kept in chemical equilibrium

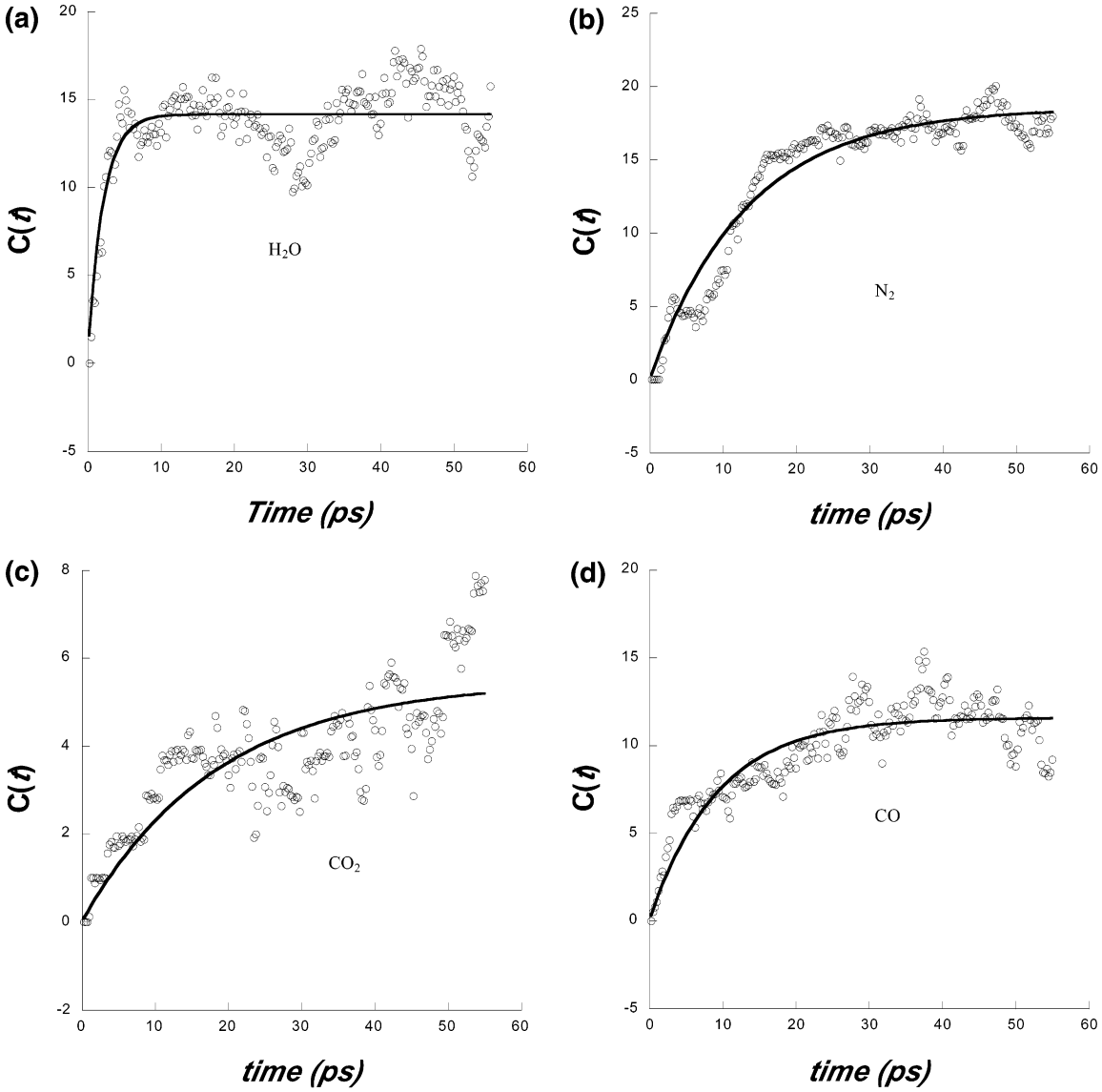

Figure 2. Product particle number formations as a function of time of (a) H_2O, (b) N_2, (c) CO_2, and (d) CO.

with the fluid phase. An explicit Gibbs free energy equation of state for carbon was used.[32] This method has been shown to be effective in predicting the equation of state of a wide variety of fluid mixtures.[33] The thermodynamic model is implemented within the Cheetah thermochemical code. For HMX, the molecules N_2, H_2O, CO_2, HNCO, and CO were predicted to be present in quantities greater than 1 mol/kg of HMX. The species CO, NH_3, H_2, CH_4, H, CH_3OH, NO, and C_2H_4 were also predicted to be present in quantities greater than 0.0001 mol/kg of HMX. The species N_2O, C_2H_2, N, O, O_2, NO_2, HCN, atomic C, and O_3 were not predicted to have significant concentrations. Carbon in the diamond phase was predicted to be in equilibrium with the other species at a concentration of 4.9 mol/kg of HMX. The thermochemical calculations predict a pressure for fully reacted HMX of 16 GPa, or 160 kbar. We note that such a pressure is achievable through shock or diamond anvil cell techniques, but not in more conventional experimental techniques.

As can be noticed in Figure 3, the results of our present simulation compare very well with the formation of H_2O, N_2, and HNCO. The relative concentration of CO and CO_2, however, is reversed at the limited time of our simulation. No condensed carbon was found in the current simulation. Several other products and intermediates with lower concentrations,

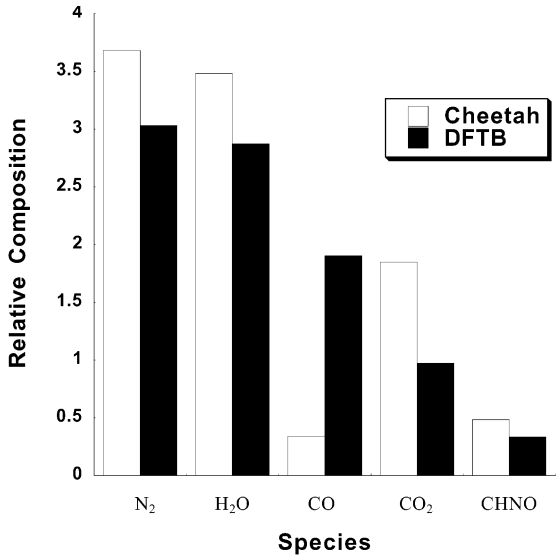

Figure 3. Comparison of relative composition of dominant species determined from current DFTB simulation (dark boxes) and from a thermodynamical calculation (empty boxes).

common to the two methods, have also been identified. These include HCN, NH_3, N_2O, CH_3OH, and CH_2O. It is hoped that interplay between the two vastly different approaches could be established at a much longer simulation time. The goal will be to expand the product molecule set of the theromochemical code with important species determined from our ab nitio based simulations for kinetic modeling.

One expects more CO_2 than CO as final products, as predicted by Cheetah (Figure 3). The results displayed in Figure 2c,d show that, at a simulation time of 40 ps, we are still in the second stage of reaction chemistry, as previously identified.[18] At this stage, the CO concentration is still rising and has not yet undergone the water gas shift reaction ($CO + H_2O \rightarrow CO_2 + H_2$) conversion. Interestingly, this shift seems to occur at around 50 ps of the simulation, with CO_2 molecules being formed as the CO concentration correspondingly diminishes. The simulation is currently being extended several more tens of picoseconds to monitor this behavior, and to eventually reach a steady state production.

The current simulation should allow for the construction of a global reaction mechanism for the decomposition of HMX at the stated physical conditions. Here, we only report the initial steps of the decomposition pathways, deferring detailed mechanisms of this and similar simulations at different conditions to future publications. The first chemical event in our simulation is the breaking of the $N-NO_2$ bond and the dissociation of NO_2 fragments. At 200 fs of simulation time, the number of NO_2 fragments is 10, out of a possible total of 24, with some being from successive elimination from the same HMX molecule. This preference to bond rupture is consistent with the recent observation that the energetic barriers for the cleavage of the $N-NO_2$ bond in the solid phase of the nitramine RDX vary depending on the location of the molecule in the crystal.[34] At this stage of the simulation, the C−N bond breaking is also exhibited, occurring in two ways: the first (1) produces methylenenitramine ($CH_2N_2O_2$), whereas the symmetric breaking (2) leads to the formation of two $C_2H_4N_4O_4$ moieties, as shown below.

Seven $CH_2N_2O_2$ species have been formed at around 200 fs of simulation time. These results are similar to those identified in thermal decomposition experiments.[2,3] A further $N-NO_2$ bond breaking then follows the decomposition (1) and (2) above. From (1), this leads to the formation of CH_2N and NO_2. These pathways are remarkably similar to those predicted previously by Melius from the decomposition of nitramines at fast heating rates.[18]

As the radical CH_2N is formed, the production of HCN occurs via the reaction:

$$CH_2N + CH_2N \rightarrow C_2H_4N_2 \rightarrow HCN + CH_2NH \qquad (I)$$

Another source for the formation of HCN follows from a series of complex reactions that also produce nitric acid, HNO_3:

$$CH_2NH + NO_2 \rightarrow CH_3N_2O_2 \qquad (II)$$

$$CH_3N_2O_2 + NO_2 \rightarrow CH_2N_2O_3 + HNO \qquad (III)$$

$$CH_2N_2O_3 \rightarrow HCN + HNO_3 \qquad (IV)$$

The schematic mechanism for these reactions is illustrated in Figure 4. We also note that formaldehyde, CH_2O, is first formed from a reaction involving large intermediate fragments. The formation occurs from the reaction of the $C_2H_4N_4O_4$ moiety, which is produced from the symmetric bond scission of the HMX molecule as in (2) above, with HNO. The reaction leads to the production of CH_2O and a larger intermediate fragment that undergoes further decomposition.

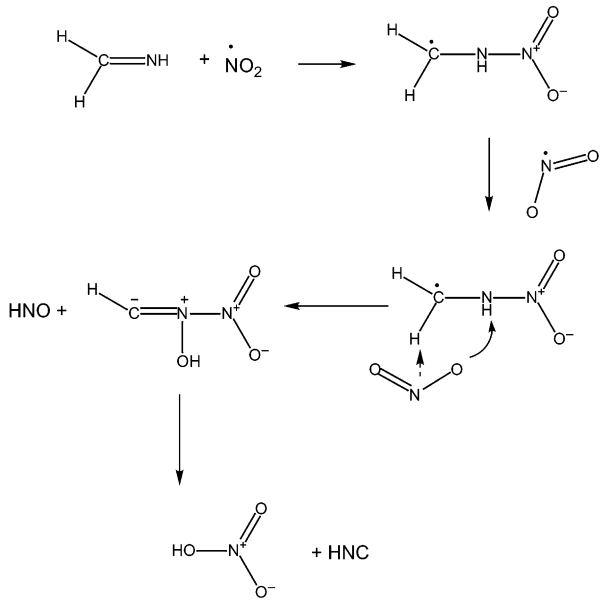

Figure 4. Mechanistic scheme for reactions I−IV responsible for the first formation of HCN.

Finally, we note that the product formation rate in our simulation is consistent with recent simulations on methane employing a similar tight-binding computational scheme.[17] It was determined that the dissociation of methane at 5000 K starts at 3 ps and evolves into a mixture of H_2 and hydrocarbon polymers after 10 ps. The composition agreed well with an earlier ab initio/molecular dynamics simulation.[15] Although tight-binding methods might overestimate reaction energy barriers, the very high temperature of the simulated system makes the free energy difference between reactants and products more important than transition state energies. The accurate determination of these reaction energies within SCC-DFTB[25] is the promising key to conduct further simulations at extreme conditions of temperature and pressure of explosive materials.

IV. Conclusion

We conducted a quantum-based molecular dynamics simulation of HMX at a density of 1.9 g/cm^3 and a temperature of 3500 K for up to 55 ps. These are conditions similar to those encountered at the Chapman−Jouget detonation state. Thus, although we do not model the entire shock process, we can provide some insight into the nature of chemical reactivity under similar conditions. Under the simulation conditions HMX was found to be in a highly reactive dense supercritical fluid state. We estimated effective reaction rates for the production of H_2O, N_2, CO_2, and CO to be 0.48, 0.08, 0.05, and 0.11 ps^{-1}, respectively. The simulation is being extended until a steady state for the production of these products is reached. The simulation can serve as a basis for the construction of a global decomposition mechanism of HMX that, lacking experimental data, can be validated through standard ab initio quantum mechanical methods. The reported results can be more fully validated through comparison with experimental findings at similar conditions, which we hope this study will motivate.

Because the SCC-DFTB method can be implemented in parallel mode[35] with great efficiency, the size of the system can be increased to a few thousand atoms without imposing severe limitations on the simulation time. Overcoming the

shortcoming of system size will allow us to consider solid carbon formation, which is not accounted for in our current simulation due to the limited system size and simulation time. The reaction rates were implemented in a three-step chemical/hydrodynamic/thermal model of flame propagation, allowing for better agreement with recent experimental results on the flame speed.[36] Further, we find reasonable agreement for the concentration of dominant species with those obtained from thermodynamic calculations.

Although the present work sheds much needed light on the chemistry of energetic materials under extreme conditions, there are methodological shortcomings that need to be overcome in the future. The demanding computational requirements of the present method limit the simulation time to less than 100 ps. In fact, the simulations reported here took over one year of simulation time on a modern workstation. This limits the method's applicability to short times and corresponding high-temperature conditions. Due to experimental difficulty, however, most work that resolves chemical speciation is done at significantly lower temperatures. A second issue is that the SCC-DFTB method is not as accurate as more elaborate ab initio methods. The high-temperature conditions of the present work ameliorate this difficulty. For instance, at 3500 K a 10 kcal/mol error in a reaction barrier leads to a factor of 4 error in the reaction rate. This is an acceptable error for qualitative study. At 600 K, however, a comparable error in the barrier would lead to a factor of 4000 error in the reaction rate. There is no quantum molecular dynamics technique currently accurate enough to provide reliable reaction rates at 600 K. Nonetheless, we find the present approach to be a promising direction for future research on the chemistry of energetic materials. The work is being extended to include several simulations at varying temperatures and densities, the results of which will be reported in future publications.

Acknowledgment. This work was performed under the auspices of the U.S. Department of Energy by the University of California, Lawrence Livermore National Laboratory, under contract No. W-7405-Eng-48. Support through the ASCI program is greatly acknowledged.

References and Notes

(1) Zel'dovich, Y. B.; Raiser, Y. P. *Physics of Shock waves and High-Temperature Hydrodynamics Phenomena*; Academic Press: New York, 1966.

(2) (a) Suryanarayana, B.; Graybush, R. J.; Autera, J. R. *Chem. Ind., London* **1967**, *52*, 2177. (b) Bulusu, S.; Axenrod, T.; Milne, G. W. A. *Org. Mass. Spectrom.* **1970**, *3*, 13.

(3) Farber, M.; Srivastava, R. D. *Proc. 16th JANNA Combust. Meeting* **1979**, *CPIA pub. 308*, 59.

(4) Morgan, C. V.; Bayer, R. A. *Combust. Flame* **1979**, *36*, 99.

(5) Fifer, R. A.In *Fundamentals of Solid Propellant Combustion, Progress in Astronautics and Aeronautics*; Kuo, K. K., Summerfield, M., Eds.; AIAA Inc.: New York, 1984; Vol. 90, p 177.

(6) Behrens, R. *J. Phys. Chem.* **1990**, *94*, 6706.

(7) Behrens, R. *Int. J. Chem. Kinet.* **1990**, *22*, 135.

(8) Behrens, R.; Bulusu, S. *J. Phys. Chem.* **1991**, *95*, 5838.

(9) Oxley, J. C.; Kooh, A. B.; Szekers, R.; Zhang, W. *J. Phys. Chem.* **1994**, *98*, 7004.

(10) (a) Brill, T. B.; Gongwer, P. E.; Williams, G. K. *J. Phys. Chem.* **1994**, *98*, 12242. (b) Brill, T. B. *J. Prop. Power* **1995**, *11*, 740.

(11) Tang, C.-J.; Lee, Y. J.; Kudva, G.; Litzinger, T. A. *Combust. Flame* **1999**, *117*, 170.

(12) Tang, C.-J.; Lee, Y. J.; Litzinger, T. A. *J. Prop. Power* **1999**, *15*, 296.

(13) Dlott, D. D. *Annu. Rev. Phys. Chem.* **1999**, *50*, 251−278.

(14) Cavazzoni, C.; Chiarotti, G. L.; Scandolo, S.; Tosatti, E.; Bernasconi, M.; Parrinello, M. *Science* **1999**, *283*, 44.

(15) Ancilotto, F.; Chiarotti, G. L.; Scandolo, S.; Tosatti, E. *Science* **1997**, *275*, 1288.

(16) Bickham, S. R.; Kress, J. D.; Collins, L. A. *J. Chem. Phys.* **2000**, *112*, 9695.

(17) Kress, J. D.; Bickham, S. R.; Collins, L. A.; Holian, B. L.; Goedecker, S. *Phys. Rev. Lett.* **1999**, *83*, 3896.

(18) Melius, C. F. *Chemistry and Physics of Energetic Materials*; Bulusu, D. N., Ed.; Kluwer: Dordercht, The Netherlands, 1990.

(19) Lewis, J. P.; Glaesemann, K. R.; VanOpdorp, K.; Voth, G. A. *J. Phys. Chem. A* **2000**, *104*, 11384.

(20) Chakraborty, D.; Muller, R. P.; Dasgupta, S.; Goddard, W. A., III. *J. Phys. Chem. A* **2001**, *105*, 1302.

(21) Smith, G. D.; Bharadwaj, R. K. *J. Phys. Chem. B* **1999**, *103*, 3570.

(22) Sorescu, D. C.; Rice, B. M.; Thompson, D. L. *J. Phys. Chem. B* **1998**, *102*, 6692.

(23) Sorescu, D. C.; Rice, B. M.; Thompson, D. L. *J. Phys. Chem. B* **1999**, *103*, 6783.

(24) Porezag, D.; Frauenheim, T.; Kohler, T.; Seifert, G.; Kaschner, R. *Phys. Rev. B* **1995**, *51*, 12947.

(25) Elstner, M.; Porezag, D.; Jungnickel, G.; Elsner, J.; Hauk, M.; Frauenheim, T.; Suhai, S.; Seifert, G. *Phys. Rev. B* **1998**, *58*, 7260.

(26) Frauenheim, T.; Seifert, G.; Elstner, M.; Hajnal, Z.; Jungnickel, G.; Porezag, D.; Suhai, S.; Scholz, R. *Phys. Status Solidi* **2000**, *217*, 41.

(27) Elstner, M.; Hobza, P.; Frauenheim, T.; Suhai, S.; Kaxiras, E. *J. Chem. Phys.* **2001**, *114*, 5149.

(28) Cui, Q.; Elstner, M.; Kaxiras, E.; Frauenheim, T.; Karplus, M. *J. Phys. Chem. B* **2001**, *105*, 569.

(29) Foulkes, W.; Haydock, R. *Phys. Rev. B* **1989**, *39*, 12520.

(30) Landers, A. G.; Brill, T. B. *J. Phys. Chem.* **1980**, *84*, 3573.

(31) Fried, L. E.; Howard, W. M. *J. Chem. Phys.* **1998**, *109*, 7338.

(32) Fried, L. E.; Howard, W. M. *Phys. Rev. B* **2000**, *61*, 8734.

(33) Fried, L. E.; Howard, W. M. *J. Chem. Phys.* **1999**, *110*, 12023.

(34) Kuklja, M. M. *J. Phys. Chem. B* **2001**, *105*, 10159.

(35) Klein, P.; Urbassek, H. M.; Frauenheim, T. *Comput. Mater. Sci.* **1999**, *13*, 239.

(36) Reaugh, J. Private communication.